A three-dimensional highly conductive structure of Si/NiSi2 anode for Li-ion battery

A three-dimensional highly conductive structure of Si/NiSi2 anode for Li-ion battery

Wurigumula Bao[1, a], Jing Wang[1, 2, 3, *], Shi Chen[1, 2, 3, b], WeiKang Li[1, c], YueFeng Su[1, 2, 3, d] and Feng Wu[1, 2, 3, e]

[1]School of Materials Science and Engineering, Beijing Institute of Technology, Beijing 100081, China
[2]Collaborative Innovation Centre for Electric Vehicles in Beijing, Beijing, 100081, China
[3]National Development Centre of High Technology Green Materials, Beijing, 100081, China

*Corresponding author e-mail: wangjingbit98@bit.edu.cn, [a]bwrgml@163.com, [b]csbit@bit.edu.cn, [c]lwk060103@163.com, [d]suyuefeng@bit.edu.cn, [e]wufeng863@vip.163.com

Abstract. The low conductivity, structural degradation during cycling and severe capacity loss in the initial cycle make silicon difficult to meet the increasing demand in various aspects as one of the promising anodes material. Here we introduce a conductive three-dimensional structure to tackle these problems. The design of the electrode is achieved via plasma enhanced chemical vapor deposition (PECVD) of silicon nanoparticles onto three-dimensional nickel foam, forming a 3D conductive network. The three-dimensional networks provide abundant electrochemical activity sites and conductive transport paths. Besides, this design can significantly improve the energy density of the electrode since no binders or conductive agents are deposited. The initial columbic efficiency of Si anode is greatly improved by tuning the deposition time. A secondary phase of $NiSi_2$ is found from XPS results which serves as an inactive buffer matrix in the composite. The anode with 40min deposition time achieves remarkable electrochemical performance as 84.84% initial columbic efficiency and 525.5mAh • g^{-1} specific capacity after the 100th cycles. This preferable performance is the result of enhanced physical and mechanical properties of the electrode with a 3D conductive structure.

1. Introduction

An increasing number of portable products such as laptops, mobile phones leads to growing demands for energy storage devices. Lithium-ion battery, with the advantage of environmentally friendly, high energy density, long cycle life, has been widely studied among all secondary batteries [1-3]. Graphite as most-used commercial anode material, with the capacity of 372mAh·g^{-1}, restricts the application of lithium-ion batteries in electric vehicles since its low energy density. Silicon is the most promising candidate because of its high theoretical capacity (3590mAh·g^{-1}), which is about 10 times the capacity of graphite [4-6]. However, the formation of $LiSi_x$ alloy during the cycle results in 300% volume expansion, inducing fragmentation of active materials and affecting cycle performance [7, 8]. In order to alleviate this volume effect, nano-tech has been introduced to silicon anodes such as nanowire, nano-porous structure and nano-array [9-11]. Besides, three-dimensional (3D) hierarchical structure

PAN/$NiSi_x$/Si electrodes have a certain degree of improvement in cycle performance and initial columbic efficiency [12]. In this paper, a three-dimensional structure Si/$NiSi_2$ anode was prepared by chemical vapor deposition, and their lithium properties were studied. This design provides abundant electrochemical activity sites and conductive transport paths, which help the electrochemical performance of silicon anode. The 40 min sample exhibited 694.9 $mAh \cdot g^{-1}$ after the 50th cycles with 84.84% initial coulombic efficiency.

2. Experimental

2.1. Preparation of Si/Ni foam electrodes

Commercial nickel foam was ultrasonically washed with acetone and then cleaned in an aqueous 0.1 M HCl solution for 30 min to remove the surface oxides. Then, the nickel foam was repeatedly rinsed with distilled water and ethyl alcohol and dried in a vacuum oven at 60°C for 1 h. Silicon was deposited onto the as-prepared nickel foams by the PECVD (Plasma-Thermal 790) method. SiH_4 gas flow as the silicon source was fixed at 500 sccm with a process pressure of 1 Torr, under the deposition power of 30W, and the processing temperature was 250°C. The deposition rate on the nickel foam was calculated to be 0.8 $mg \cdot cm^{-2} \cdot h^{-1}$, and the deposition time was varied from 20min to 100min.

2.2. Material characterization and electrochemical measurements

XRD was characterized using Rigaku Ultima IV-185 X-ray diffractometer (Cu-Ka radiation, l ¼ 1.5406 A, 40 kV, and 40 mA) at a scan rate of 2 min^{-1}. SEM was performed on a Zeiss SUPRA 55 microscope equipped with a Phoenix EDX spectrometer. XPS spectra were obtained using a Kratos AXIS-165 Surface Analysis System with a monochromatic Al Ka source.

The electrochemical measurements were carried out using 2032 coin-type half-cells. Lithium metal was served as the counter electrode, and 1 M $LiPF_6$ in a solvent mixture of ethylene carbonate (EC)/dimethyl carbonate (DMC) (1:1 by volume) with 5 vol% FEC acted as the electrolyte. The cells were assembled in an argon-filled glove box. Cyclic voltammetry (CV) and electrochemical impedance spectroscopy (EIS) tests were performed on a Chi660E electrochemical workstation. Galvanostatic charge-discharge tests were carried out using a Land CT2001A battery tester. The capacity and current density were calculated from the total weight of Si.

3. Results and discussion

3.1. Structure and Morphology

The XRD patterns of the electrodes are shown in Fig. 1b'. All composites show three sharp diffraction peaks (44.58°, 51.88°, and 76.48°), which can be indexed to the Ni metal with a single-phased face-centered cubic structure [13]. No peaks related to oxides can be found, indicating that the Si is primarily amorphous [14]. As the deposition time becomes longer, the peak intensity decreases, indicating that more silicon is deposited on the nickel surface.

Fig. 1a shows the scanning electron microscopy (SEM) image of the pristine Ni substrate, displaying a three-dimensional interconnected porous structure with internal space of 200-300μm. Many bumps and gaps on the surface of the nickel foam can be found after acid treatment, which provides a growth template for subsequent silicon. These bumps also increase the contact area of the active materials with the current collector. Fig. 1(b-f) show the images of the as-prepared electrode with different deposition time at 20min, 40min, 60min, 80min, and 100min, respectively. The surface of the electrode still has bumps after 20min deposition and as the deposition time increases, the surface becomes flat. In addition, Fig. 1(h–l) exhibit the surface elemental distribution of the 40min sample. The EDS elemental mapping revealed the uniformity of Si elemental on the whole foam network.

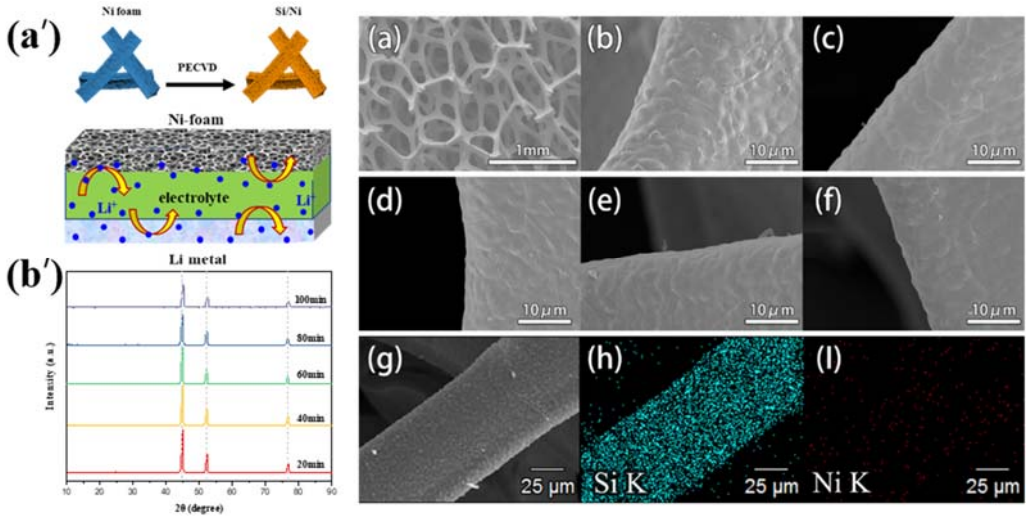

Figure 1. (a') fabrication process of $Si/NiSi_2$ electrodes, (b') XRD patterns of $Si/NiSi_2$ electrodes. SEM images of the pure Ni foam (a), 20min (b), 40min (c), 60min (d), 80min (e), and 100min (f) electrodes. SEM image (g) and corresponding EDS elemental mapping (h–l) of the 40min electrode

The details of the as-synthesized Si-based anodes were further carried out by XPS, as shown in Fig. 2. In Si 2p spectra, the fitting peak at 103.5 eV is attributed to SiO_2, while the satellite peak at 99.4 eV is related to Si [15, 16]. This may be partial Si has undergone a redox reaction with NiO into SiO_2 due to that nickel reacts easily with oxygen in the air to form a dense layer [16]. In the Ni 2p spectra, a Ni 2p peak centered at 854.6 eV (Ni 2p3/2), which indicate the presence of $NiSi_2$ phase along with Si [17]. The peaks appeared at 861.1 eV (Ni2p3/2) attributed to NiO [18]. Accordingly, the results of XPS data confirms the presence of NiO and $NiSi_2$.

3.2. Electrochemical performance

As shown in Fig. 2c. The 100min electrode delivered a high initial discharge capacity of 3332.5mAh·g^{-1}, however, the capacity was dramatically decreased in the subsequent cycles. The 40min electrodes exhibited great improvements in the cycle performance. It delivered 525.5mAh·g^{-1} after 100 cycles. Note that the cycle performance of the composite electrodes was gradually decreased as the deposition time increased from 40min to 100min. This suggested an optimization deposition time in the electrode. The more silicon deposited on Ni foam, the worse the conductivity of the electrode. In contrast, when the Si layer cannot cover the current collector, the collector will be exposed to the electrolyte and more side reactions occur. Fig. 2d is the columbic efficiency of the electrodes. It can be seen that the efficiency of 80min and 100min electrodes fluctuates greatly, the volume expansion of Si during cycling results in the loss of capacity. Meanwhile, the irreversible intercalation reaction of NiO also leads to the attenuation of the performance. In contrast, the efficiency of 40min is more stable, which indicates that the electrode with this deposition time not only ensures the conductivity but also have appropriate voids to alleviate the volume expansion of Si. The 40min electrode exhibits an excellent rate performance as well. Fig. 2e shows that the capacity reposefully declines from 3230.1mAh·g^{-1} to 538mAh·g^{-1} when the current rate increases in stages from 0.1C to 3C, and still remains nearly 1449.1mAh·g^{-1} at 0.1C. Obviously, the superior rate capability of the 40min electrode benefits from the unique anode structure with a 3D framework, which increases the electronic transport between active materials and the current collector, the existence of conductive crystalline $NiSi_2$ also enhancing the electronic conductivity.

Fig. 2f shows the cyclic voltammetry of the 40min electrode at a scan rate of 0.1 mV·s^{-1}. The electrode appeared a broad weak cathodic peak between 0.02V-0.75 V, which could correspond to the reductive decomposition of the electrolyte and the subsequent formation of SEI layers on the surface of active materials. The cathodic peak at about 0.02 V corresponded to the alloying of Si with Li [19]. In

the following half cycle, an obvious anodic peak appeared at 0.39V and 0.51 V, representing the dealloying of the Li-Si alloys [20]. During the second cathodic sweep, a new reduction peak was observed at 0.13 V, which is likely to be a two-stage alloying reaction of Li^+ with the $NiSi_2$/Si phase, which contains the formation of two different lithiated states [21]. It is worth noting that a small cathodic peak is located at 1.21V for the first cycle owing to the lithiation of NiO [22], but the anodic peak is not observed and no other related redox peaks are observed in subsequent cycles, suggesting the irreversible lithiation of NiO, which is consistent with the XPS results.

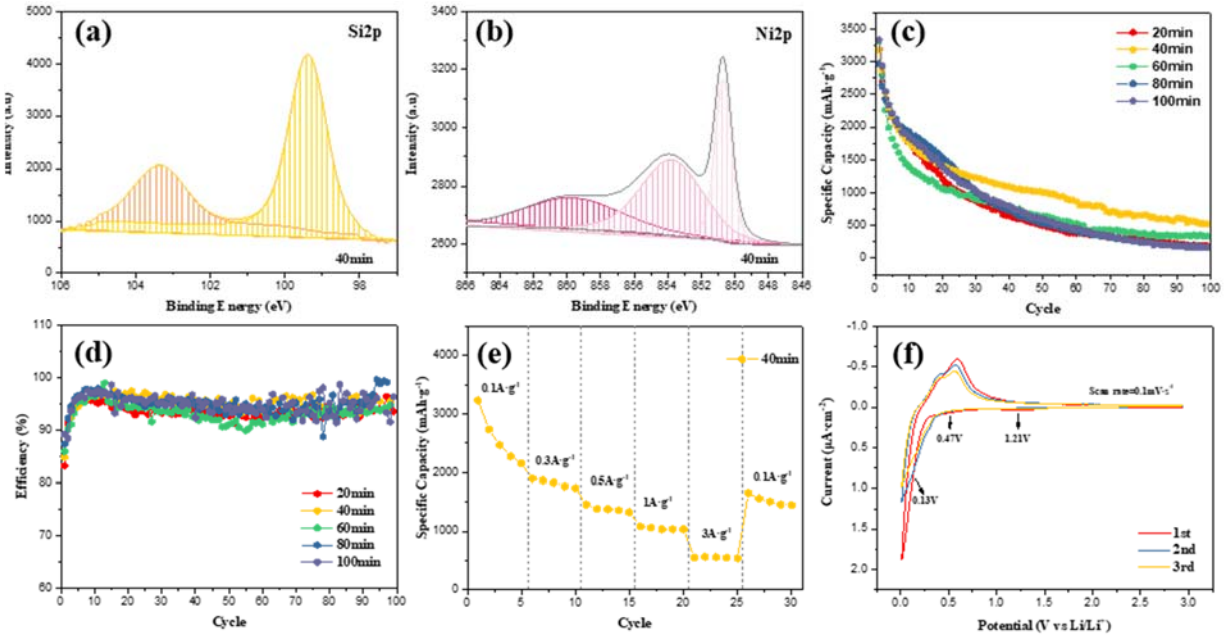

Figure 2. High-resolution XPS spectra of Si 2p (a) and Ni 2p (b) for the 40min electrode. (c) Cycling performance and (d) corresponding CE of the different Si deposition time electrodes. (e) Rate capability of the 40min electrodes at different current densities. (f) CV of the 40min electrode.

The voltage profiles of the Galvano static charge/discharge cycling at different deposition time are presented in Fig. 3(a-d). The irreversible capacity loss during the first lithiation process can be mainly attributed to the formation of the solid electrolyte interphase (SEI) on the surface of the electrode. In Fig. 3a, the 20min composite shows a new reaction platform nearly 1.5V, which corresponds to the lithiation of NiO [23]. From the second cycle, the new platform disappeared, which means the lithiation of NiO is an irreversible reaction since NiO is reduced to nickel when charged and metal nickel is inactive for lithium. The reaction at 1.5V only occurs in Fig. 3a and Fig. 3b, because the silicon deposition layer was not thick enough to prevent the reaction.

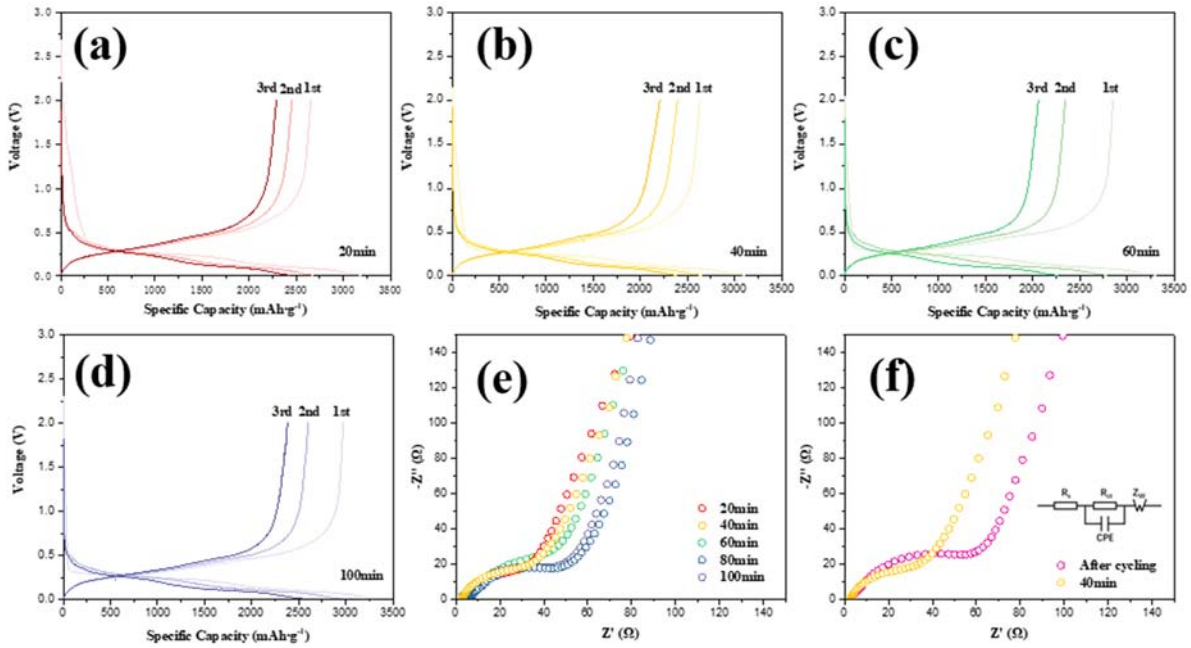

Figure 3. Voltage profiles of the 20min (a), 40min (b), 60min (c) and 100min (d) electrodes. (e) Electrochemical impedance spectral profiles of the different Si deposition time electrodes before cycling, and (f) Nyquist plots of the 40min electrode before and after 50 cycles

Fig. 3e shows the electrochemical impedance spectra profiles of the 40min electrodes at open circuit potential. The semicircle indicated the charge transfer resistance (R_{ct}) and double-layer capacitance (C_{dl}), and the sloping line represented the Warburg impedance (Z_w) associated with lithium-ion diffusion in the bulk electrode [24]. It is obvious that the 100min electrode showed the maximal R_{ct}, and the 20min electrode showed the minimal R_{ct}. As the amount of deposition increases, the conductivity of the electrode is reduced because of the poor conductivity of silicon. Fig. 3f illustrated the electrochemical impedance spectra profiles of the 40min electrode before and after cycling. The R_s had no obvious change, but the R_{ct} slightly increased. Such a slow increase in R_{ct} upon cycling indicates a relatively stable electrode-electrolyte interface and therefore good cycle performance of the composite electrode. This signifies the enhanced electronic conductivity of the Si electrode, which is bridged by continuous conductive networks.

4. Conclusion

In conclusion, we have developed 3D conductive network Si anode material via a PECVD method with optimized performance in terms of reversible specific capacity, cyclability, and rate capability. Nickel foam as a 3D network conductive support provides a fast transmission path for electrons, increasing the reversibility of the reaction. The $NiSi_2$ phase can be mainly considered as an inactive component, serves as a buffer zone to effectively accommodate the volume changes of silicon during lithiation/delithiation. The as-prepared electrode displayed a stable specific capacity of 694.9 $mAh \cdot g^{-1}$ for 50 cycles at 0.1C and good rate capability. In addition, the synthesis route developed in this work is very simple, which is in turn also possible to be used for the preparation of other silicon alloy composites with an improved cycling stability and rate performance.

Acknowledgments

This work was financially supported by the National Key R&D Program of China [grant number 2018YFB0104401].

References

[1] Q. Xu, J.K. Sun, Z.L. Yu, Y.X. Yin, S. Xin, S.H. Yu, Y.G. Guo, SiO x Encapsulated in Graphene Bubble Film: An Ultrastable Li-Ion Battery Anode, Advanced Materials, (2018) e1707430.
[2] C. Wang, H. Wu, Z. Chen, M.T. McDowell, Y. Cui, Z.A. Bao, Self-healing chemistry enables the stable operation of silicon microparticle anodes for high-energy lithium-ion batteries, Nat Chem, 5 (2013) 1042 - 1048.
[3] N. Nitta, F.X. Wu, J.T. Lee, G. Yushin, Li-ion battery materials: present and future, Mater. Today, 18 (2015) 252 - 264.
[4] J. Wang, M.J. Zhou, G.Q. Tan, S. Chen, F. Wu, J. Lu, K. Amine, Encapsulating micro-nano Si/SiOx into conjugated nitrogen-doped carbon as binder-free monolithic anodes for advanced lithium ion batteries, Nanoscale, 7 (2015) 8023 - 8034.
[5] Y.M. Sun, N.A. Liu, Y. Cui, Promises and challenges of nanomaterials for lithium-based rechargeable batteries, Nature Energy, 1 (2016).
[6] S.J. Park, H. Zhao, G. Ai, C. Wang, X.Y. Song, N. Yuca, V.S. Battaglia, W.L. Yang, G. Liu, Side-Chain Conducting and Phase-Separated Polymeric Binders for High-Performance Silicon Anodes in Lithium-Ion Batteries, Journal of the American Chemical Society, 137 (2015) 2565 - 2571.
[7] J. Chang, X. Huang, G. Zhou, S. Cui, P.B. Hallac, J. Jiang, P.T. Hurley, J. Chen, Multilayered Si nanoparticle/reduced graphene oxide hybrid as a high-performance lithium-ion battery anode, Adv Mater, 26 (2014) 758 - 764.
[8] Z. Chen, C. Wang, J. Lopez, Z.D. Lu, Y. Cui, Z.A. Bao, High-Areal-Capacity Silicon Electrodes with Low-Cost Silicon Particles Based on Spatial Control of Self-Healing Binder, Advanced Energy Materials, 5 (2015).
[9] S. Li, J.J. Niu, Y.C. Zhao, K.P. So, C. Wang, C.A. Wang, J. Li, High-rate aluminium yolk-shell nanoparticle anode for Li-ion battery with long cycle life and ultrahigh capacity, Nat. Commun., 6 (2015) 7.
[10] D.C. Lin, Z.D. Lu, P.C. Hsu, H.R. Lee, N. Liu, J. Zhao, H.T. Wang, C. Liu, Y. Cui, A high tap density secondary silicon particle anode fabricated by scalable mechanical pressing for lithium-ion batteries, Energy Environ. Sci., 8 (2015) 2371 - 2376.
[11] Y.Z. Li, K. Yan, H.W. Lee, Z.D. Lu, N. Liu, Y. Cui, Growth of conformal graphene cages on micrometre-sized silicon particles as stable battery anodes, Nature Energy, 1 (2016).
[12] W. Bao, J. Wang, S. Chen, W. Li, Y. Su, F. Wu, G. Tan, J. Lu, A three-dimensional hierarchical structure of cyclized-PAN/Si/Ni for mechanically stable silicon anodes, J Mater Chem A, (2017).
[13] J. Liu, N. Li, M.D. Goodman, H.G. Zhang, E.S. Epstein, B. Huang, Z. Pan, J. Kim, J.H. Choi, X. Huang, Mechanically and chemically robust sandwich-structured c@si@c nanotube array li-ion battery anodes, Acs Nano, 9 (2015) 1985.
[14] K. Ogata, E. Salager, C.J. Kerr, A.E. Fraser, C. Ducati, A.J. Morris, S. Hofmann, C.P. Grey, Revealing lithium-silicide phase transformations in nano-structured silicon-based lithium ion batteries via in situ NMR spectroscopy, Nat. Commun., 5 (2014) 3217.
[15] S.O. Kim, A. Manthiram, A facile, low-cost synthesis of high-performance silicon-based composite anodes with high tap density for lithium-ion batteries, J Mater Chem A, 3 (2015) 2399 - 2406.
[16] C.C. Nguyen, T. Yoon, D.M. Seo, P. Guduru, B.L. Lucht, Systematic Investigation of Binders for Silicon Anodes: Interactions of Binder with Silicon Particles and Electrolytes and Effects of Binders on Solid Electrolyte Interphase Formation, Acs Appl Mater Inter, 8 (2016) 12211-12220.
[17] Y. Cao, L. Nyborg, U. Jelvestam, XPS calibration study of thin-film nickel silicides, Surface and Interface Analysis, 41 (2009) 471 - 483.
[18] I. Preda, R.J.O. Mossanek, M. Abbate, L. Alvarez, J. Méndez, A. Gutiérrez, L. Soriano, Surface contributions to the XPS spectra of nanostructured NiO deposited on HOPG, Surface Science,

606 (2012) 1426 - 1430.
[19] B. Li, F. Yao, J.J. Bae, J. Chang, M.R. Zamfir, D.T. Le, D.T. Pham, H. Yue, Y.H. Lee, Hollow carbon nanospheres/silicon/alumina core-shell film as an anode for lithium-ion batteries, Scientific Reports, 5 (2015).
[20] C.K. Chan, H. Peng, G. Liu, K. McIlwrath, X.F. Zhang, R.A. Huggins, Y. Cui, High-performance lithium battery anodes using silicon nanowires, Nat Nanotechnol, 3 (2008) 31-35.
[21] D. Zhou, H. Jia, J. Rana, T. Placke, R. Klöpsch, G. Schumacher, M. Winter, J. Banhart, Investigation of a porous NiSi 2 /Si composite anode material used for lithium-ion batteries by X-ray absorption spectroscopy, Journal of Power Sources, 324 (2016) 830 - 835.
[22] J. Wang, W. Bao, L. Ma, G. Tan, Y. Su, S. Chen, F. Wu, J. Lu, K. Amine, Scalable Preparation of Ternary Hierarchical Silicon Oxide-Nickel-Graphite Composites for Lithium-Ion Batteries, ChemSusChem, 8 (2015) 4073 - 4080.
[23] J. Ma, L. Yin, T. Ge, 3D hierarchically mesoporous Cu-doped NiO nanostructures as high-performance anode materials for lithium ion batteries, CrystEngComm, 17 (2015) 9336-9347.
[24] F. Wu, W. Li, L. Chen, Y. Lu, Y. Su, W. Bao, J. Wang, S. Chen, L. Bao, Polyacrylonitrile-polyvinylidene fluoride as high-performance composite binder for layered Li-rich oxides, Journal of Power Sources, 359 (2017) 226 - 233.